Journal of Materials Chemistry B

Accepted Manuscript

ROYAL SOCIETY OF CHEMISTRY

www.rsc.org/materialsB

Journal of Materials Chemistry B RSCPublishing

PAPER

Photothermal Effect of Silica-Carbon Hollow Sphere-Concanavalin A for Liver Cancer Cells

Cite this: DOI: 10.1039/xoxxoooooox

Ying-Chi Chen,[a] Wen-Tai Chiu,[*ab] Jung-Chih Chen,[c] Chia-Sheng Chang,[d] Lily Hui-Ching Wang,[e] Hong-Ping Lin[*df] and Hsien-Chang Chang[*abf]

Received ooth January 2012,
Accepted ooth January 2012

DOI: 10.1039/xoxxoooooox

www.rsc.org/

Hepatocellular carcinoma (HCC) is one of the most common cancers and causes of death by cancer. Concanavalin A (ConA) lectin can specifically bind to the glycoprotein receptors of HCC, which are produced by the aberrant overexpression of liver cancer cells. ConA was used in the current study to conjugate on silica-carbon hollow spheres (SCHSs) and applied in the thermal ablation therapy of liver cancer cell lines under near-infrared (NIR) laser irradiation. We found that the amount of ConA-SCHSs complex binding to hepatoma cells was significantly higher than that seen with normal hepatocyte, based on flow cytometric analysis and confocal imaging. Hepatoma cells incubated with ConA-SCHSs were thus more easily killed by the subsequent irradiation with a NIR laser. The results show that the ConA-SCHSs complex may enhance the interaction with highly expressed ConA receptors on hepatoma cells, and thus serve as an effective photothermal therapy agent for liver cancer treatment.

1. Introduction

Hepatocellular carcinoma (HCC) remains the fifth most common cancer and the fourth most common cause of cancer death in the world.[1] Although there has been notable progress in the development of cancer therapy, such as liver transplantation, surgical resection, transarterial embolization /chemoembolization, hormonal therapy, and chemotherapy,[2] the death rate from liver cancer remains high due to the low efficacy of conventional strategies. Compared to traditional cancer therapy, photodynamic therapy (PDT) is a noninvasive surgical technology with minimal side effects, in which singlet oxygen is used to kill the cancer cells.[3-6] However, the disadvantage of most photosensitizers is that they are easily affected by the environmental ambient light *in vitro*, which can cause unwanted off-target activation. In addition, the hydrophobic aromatic domains of PDT sensitizers can form aggregate that lead to self-inactivation in aqueous surroundings. Photothermal therapy (PTT) for the treatment of cancer has recently become a feasible alternative,[7-9] in which the target cells are heated.[10,11] Near-infrared (NIR) light-induced PTT is an emerging field of anticancer therapy, because light at this wavelength can penetrate deeper into the tissues, with significantly less interference from autofluorescence.[12] There are two ranges of wavelengths, called bio-windows, that can be used for this in the near-infrared range which are 650-950 nm (the first bio-window) and 1000-1350 nm (the second bio-window).[13]

The glycans on tumor cells have been shown to have abnormal structures, which alter the activity of the enzymes involved in the glycosylation reaction. Overexpression of glycotransferases in cancer cells contributes to glycan accumulation and the development of abnormal glycan structures. Furthermore, aberrant glycosylation in cancer cells promotes complex branching patterns of glycans compared to those seen in normal cells.[14] Concanavalin A (ConA), a lectin, isolated from *Canavalia ensiformis* (Jack bean) that can specifically bind to glycoproteins on the cell surface, has a high affinity to the mannose and glucose on glycoproteins. The amount of glycosylated glycoproteins on the surface of cancer cells is greater than that on normal cells, because abnormal and aberrant glycosylation often occurs in cancer cells. This indicates that the binding capacity of ConA to cancer cells may greater than that to normal cells, and thus ConA may be a potential targeting agent for anticancer therapy.[15-18]

Recent advances in nanomaterials have produced substances with excellent physical, chemical, and biological properties and high surface area to volume ratios, such as those seen with gold[19-21] and carbon nanomaterials.[22-24] An ideal light absorbing agent for cancer therapy must have a high degree of absorption in the NIR region, so that it can absorb light to produce heat in PTT for tumor ablation. Among the potential materials that have been produced, carbon black and silica nanomaterials have the advantages of low cost and cytotoxicity,[25,26] as well as being easy to obtain and fabricate compared to other metal nanomaterials. Carbon black can absorb NIR to produce heat and silica can be used to construct hollow spheres with a microstructure that prevents heat loss, enabling the hollow spheres to be maintained at high temperatures for a long time. According to our previous work we thus used hollow spheres made of carbon black and silica to perform PTT for live cancer cells.[27]

In this study we demonstrate that the combination of ConA and silica-carbon hollow spheres (SCHSs) can be used with NIR irradiation to efficiently kill liver cancer cells *in vitro*.

2. Experimental section

2.1. Chemicals

ConA and FITC labeled ConA (ConA-FITC) were purchased from Sigma-Aldrich. High glucose Dulbecco's Modified Eagle's Medium (DMEM), Dulbecco's Modified Eagle's Medium/Ham's F-12 Mixture (DMEM/F12), phosphate buffered saline (PBS), the antibiotics penicillin and streptomycin, and trypsin were purchased from Caisson. Hoechst 33342, trypan blue and paraformaldehyde were purchased from Molecular Probes, Corning and Alfa Aesar, respectively.

2.2. Synthesis of the silica-carbon hollow spheres

A stable gelatin-modified poly(methyl methacrylate) (PMMA) bead colloid solution was prepared by dissolving 0.15 g of gelatin and 0.5 g of PMMA beads with a diameter of around 300 nm in 25 mL under stirring for 1 hr. An acidified silicate solution at pH 4.0 was then added to the gelatin-PMMA bead solution. The acidified silicate solution was obtained from a simple mixing of 20 g of 3.0 wt% sodium silicate solution and 20 g of 0.15 M H_2SO_4, pH fine-tuning to 4.0 and aging for 5 mins. A silica-gelatin-PMMA beads gel solution was thus formed. After stirring for few hrs, the gel solution was hydrothermally treated at 100°C for 1 day. Filtration and drying produced the silica@PMMA beads. To produce the carbon-silica hollow spheres, the silica@PMMA beads were then pyrolyzed at 800°C for 1 hr under a helium atmosphere.

2.3. Characterization of SCHSs

The size and morphology of SCHSs were analyzed by using scanning electron microscopy with energy-dispersive spectroscopy (SEM-EDS) capabilities (SEM, JSM-6700F, JEOL), and transmission electron microscopy (TEM) images were taken with a Hitachi S-7500 at an accelerating voltage of 80 kV. The SEM experiments were performed with a Hitachi S-4800 by using an accelerating voltage of 5 or 10 kV. The thermogravimetric analysis was carried out on TA Q50 from 100-800°C at a heating rate of 30°C/min under an air atmosphere.

2.4. Temperature response of SCHSs in solution

SCHSs were diluted to different concentrations with high glucose DMEM. 100 μL of different concentrations (50-1000 μg/mL) of SCHSs solutions were then added into a 96-well plate and exposed to an 808 nm NIR laser at a power level of 250 mW (~1.23 W/cm^2) for 10 mins. The temperature was measured with a thermocouple.

2.5. Preparation of ConA(-FITC)-SCHSs

Sonication was performed to prevent aggregation of SCHSs before each experiment, then the SCHSs solution was mixed with different concentrations of ConA(-FITC) at room temperature for 12 hrs with rotation. Finally, the ConA(-FITC)-SCHSs complexes were obtained by centrifugation and washed three times by PBS.

2.6. Cell culture

Human liver cancer cells (HuH-7) and mouse liver cancer cells (ML-1) were cultured in high glucose DMEM supplemented with 10% fetal bovine serum and the antibiotics penicillin/streptomycin; the hTERT gene transformed human neonatal hepatocyte cells (NeHepLxHT)[28] were cultured in high glucose DMEM/F-12 supplemented with 10% fetal bovine serum, the antibiotics penicillin/streptomycin, 100 nM dexamethasone, 0.1% ITS premix, 20 ng/mL human EGF and 5 μg/mL ciprofloxacin. All cells were maintained at 37°C under 5% CO_2 in a humidified incubator.

2.7. Confocal imaging

2×10^4 cells were seeded in 35-mm cover glass-bottom dish overnight then incubated with ConA-FITC-SCHSs for 12 hrs. PBS washing was carried out three times to remove unbounded ConA-FITC-SCHSs, and cells were fixed in ice-cold 4% paraformaldehyde for 15 mins. Paraformaldehyde was removed by washing out with PBS for six times, and immunofluorescence images were obtained using an Olympus FluoView laser scanning confocal microscope (FV1000, Tokyo, Japan) with a 488 nm laser.

2.8. Cell viability

2×10^5 cells were seeded in a 35-mm dish for 24 hrs, then cells were treated with different concentrations of ConA-SCHSs (the relative concentrations of ConA:SCHSs were 125:50 or 250:100 μg/mL) for various reaction times (6-24 hrs). The blue fluorescent dye Hoechst 33342 was used to calculate the relative cell viability between treated and untreated cells.[29]

2.9. Flow cytometry

Flow cytometric analysis was performed by using a FACS Calibur flow cytometer (BD), and the Winmdi software was used to analyze the fluorescence signal. The amount of ConA:SCHSs in the cells was calculated by the intensity of fluorophore FITC (fluorescein isothiocyanate), which had been covalently conjugated with ConA.

2.10. Photothermal therapy

5×10^4 cells were seeded in a 24-well plate overnight and then incubated with ConA-SCHSs (the relative concentrations of ConA:SCHSs were 125:50 or 250:100 μg/mL) for 12 hrs. After ConA-SCHSs incubation, cells were washed three times with PBS and then incubated in 1 mL phenol red-free medium. After that, cells were exposed to 808 nm NIR laser at different power levels: 100 mW (~0.49 W/cm^2), 150 mW (~0.74 W/cm^2), 200 mW (~0.99 W/cm^2) and 250 mW (~1.23 W/cm^2) for 5 mins. Trypan blue staining was used to differentiate dead cells from live cells. The cell viability was calculated by measuring the percentage of lethal area (positive trypan blue staining) in the laser spot area.

2.11. Statistical analysis

Mean and standard deviations were calculated by the Student's *t*-test for multiple comparisons ($n \geqq 3$). All data are represented as mean±SEM (standard error of the mean) in each experiment. Student's *t*-test was used for statistical analyses, with a *p* value

< 0.05 considered significant (*: $p<0.05$; **: $p<0.01$; ***: $p<0.001$).

3. Results and discussion

3.1. Morphology of silica-carbon hollow spheres

Fig. 1A shows schematic illustrations of a 3D model (upper panel) and 3D cross section (lower panel) of SCHSs. The SEM images in Fig. 1B show distinct silica-carbon spheres with a uniform size of about 300 nm in diameter, with hollow interiors seen in a very few broken ones. The TEM images show a shell thickness of around 15-20 nm (Fig. 1C). SEM-EDS analysis was performed in order to confirm composition of the SCHSs. As shown in Supporting Information Fig. S1, the SCHSs are composed of silicon, oxygen and carbon elements. The N_2 adsorption-desorption isotherm of the SCHSs was shown in Fig. S1B.

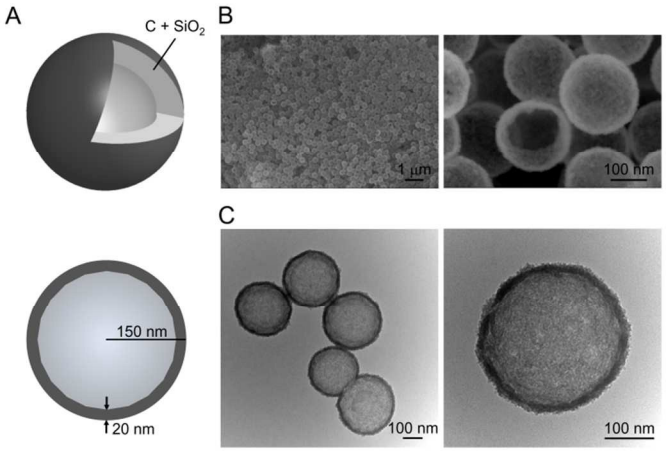

Fig. 1 (A) Schematic of a 3D model (upper panel) and cross section (lower panel) of SCHSs. Images of SCHSs obtained by (B) scanning electron microscopy (SEM) and (C) transmission electron microscopy (TEM) show the hollow sphere structure. The average diameter of SCHSs is around 300 nm.

The simple approach to synthesize mesoporous SCHSs involves the adaptation of the surface-interaction between gelatin and PMMA beads. In practice, gelatin containing either hydrophilic or hydrophobic amino acids is a very effective in preventing the aggregation of PMMA beads. In addition, gelatin can also act as gelation template for the mesoporous silica at pH of 4.0. The high fidelity of the silica replicas indicates that the interactions at the surface of the gelatin-activated PMMA beads are strong enough to be stable throughout the silica condensation, and that the silicification on the template (i.e., interfacial recognition) is competitive over the analogous process in bulk solution. Because of the high thermal stability of the mesoporous silica shell, the PMMA and gelatin were carbonized on the mesoporous silica surface without fracturing the silica cast. Consequently, we provide a convenient method to prepare uniform SCHSs by using a natural gelatin polymer as the mesostructural template and surface activation agent, sodium silicate as the silica source, and commercially available PMMA beads as the hard template. The proposed formation mechanism of the mesoporous SCHSs was illustrated in Fig. S1C.

Previous studies indicated that the size and surface modification of nanomaterials could affect the cellular uptake and cell viability.[25,26,31] Here, the SCHSs used in this study showed biocompatibility and no cytotoxicity on hepatocyte and hepatoma cells (Fig. S3).

3.2. Thermal analysis of silica-carbon hollow spheres

The TGA curve of the SCHSs sample is shown in Fig. 2A, and it can be seen that there is about a 12 wt% weight loss that occurs from 550°C to 700°C, and the carbon content and the carbon/silica weight ratio in the SCHSs is about 0.136. In addition, the high combustion temperature indicates the high thermal stability of the SCHSs. SCHSs are thus especially attractive for use in PTT, based on their simple fabrication and high absorption efficiency of NIR energy. A distinct concentration-dependent temperature raise was observed for the SCHSs solution under laser irradiation, as shown in Fig. 2B. Significantly, the solution (medium) temperature rose from 28.5°C to 54.0°C when 1000 μg/mL SCHSs solution was exposed to an 808 nm NIR laser at the power level of 250 mW (~1.23 W/cm^2) for 10 mins, whereas control solution (medium) without SCHSs showed no difference in temperature, confirming that SCHSs could act as an efficient photothermal agent.

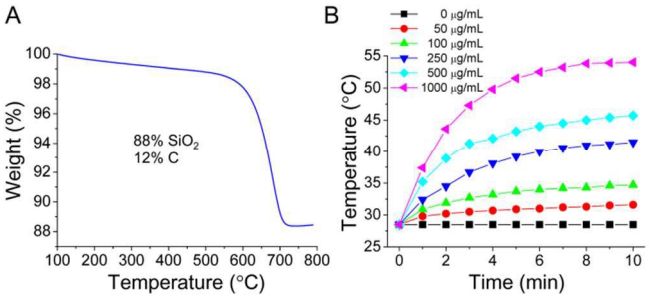

Fig. 2 Composition and thermal effect of the SCHSs. (A) Thermogravimetric analysis (TGA) curve of the SCHSs. About 88% of silica (SiO_2) was retained at a temperature of 800°C. (B) The temperature rising curves of media with different concentrations (50-1000 μg/mL) of SCHSs.

This study has demonstrated that the ConA conjugated SCHSs killed liver cancer cells efficiently through the photothermal effect. The ratio of ConA to SCHSs affected the binding capacity of ConA-SCHSs with regard to the cells, and its anti-cancer photothermal effect. Moreover, the levels of SCHSs on/in cells also affected the temperature response and photothermal cancer ablation capacity *in vitro*. However, the thermal effectiveness of SCHSs was based on the proportion of carbon material, with TGA and SEM-EDS being used to analyze this. The results of TGA and SEM-EDS showed that the proportion of carbon in our SCHSs was 12% and 28%, respectively, and this inconsistency may be because carbon is a light element, and thus less X-rays were produced, and the EDS detector could not fully detect the photon energy.[30] While SEM-EDS may not be the most effective tool for element analysis, it was able to confirm that SCHSs were made of silicon (Si), oxygen (O) and carbon (C), as shown in Fig. S1.

The photothermal efficiency of SCHSs showed perfect NIR absorbing capacity in the medium, as shown in Fig. 2B. Our data also revealed that the SCHSs can be used as an effective NIR photothermal agent to kill the cancer cells *in vitro*, as shown in Figs. 5 and 6.

3.3. The binding capacity of ConA-FITC-SCHSs and liver cancer cells

The ConA-FITC binding capacity of SCHSs was first measured at a fixed concentration of SCHSs with different concentrations of ConA-FITC using flow cytometry. Fig. S2A shows the corresponding fluorescence histograms of different concentrations of ConA-FITC-SCHSs (0:10-50:10 μg/mL), and a gradual increase in the peak fluorescence can be clearly seen. This indicates that the binding capacity of SCHSs to ConA-FITC is proportional to the ConA-FITC's levels. In addition, there was no significant difference at different reaction time points (1-24 hrs; Fig. S2B). We thus chose 1 hr as the optimal incubation time for physical conjugation of SCHSs and ConA-FITC in the following experiments. On the other hand, Fig. S2C shows that ConA-FITC binds to ML-1 cells in a dose-dependent manner (1-50 μg/mL). However, there was no significant difference between groups of 25 μg/mL and 50 μg/mL ConA-FITC, because both doses reached the maximal capacity to bind ML-1 cells. 25 μg/mL ConA-FITC was thus used in following experiments, and the optimal ratio of ConA-FITC:SCHSs is 25:10 μg/mL.

In order to find the optimal concentrations of ConA-FITC:SCHSs to interact with ML-1 liver cancer cells, various concentrations of ConA-FITC with SCHSs ranging from 25:10 to 250:100 μg/mL were tested in this study. As shown in Fig. 3B, the binding between ConA-FITC:SCHSs and ML-1 cells occurs in a dose-dependent manner, with the 250:100 μg/mL concentration of ConA-FITC with SCHSs having the highest binding capacity (15.3-fold compared to the control group) with regard to ML-1 cells. Moreover, the incubation time (1 to 18 hrs) for the ConA-FITC:SCHSs and ML-1 cells interaction is time-dependent (Fig. 3A). The optimal incubation time needed to reach the maximal binding between ConA-FITC:SCHSs and ML-1 cells is 12 hrs (30.8-fold compared to the control group). The 250:100 μg/mL concentration of ConA-FITC with SCHSs in order to form ConA-FITC:SCHSs , incubated with ML-1 cells for 12 hrs, was thus used in the following experiments.

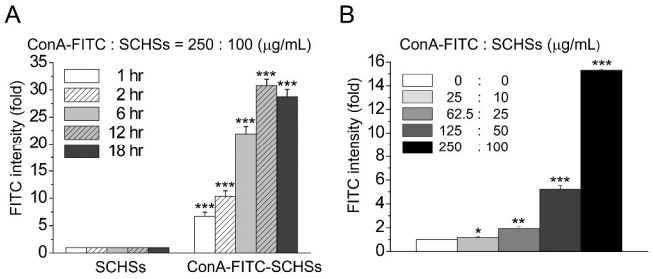

Fig. 3 The binding capacity between nanospheres and cells. Flow cytometric analysis was used to measure the binding capacity of ML-1 cells with ConA-FITC-SCHSs at (A) different incubation times (1-18 hrs) and (B) various ConA-FITC to SCHSs concentrations (25:10-250:100 μg/mL). Each column represents mean±SEM from at least three independent experiments. P values were calculated by the Student's t-test: *, $p<0.05$; **, $p<0.01$; ***, $p<0.001$.

3.4. Cytotoxicity of ConA-SCHSs on normal and cancerous liver cells

The ideal photothermal materials for biological applications should be biocompatible and non- or low-toxic. A Hoechst 33342 staining assay was used to quantitatively estimate the cytotoxic effects of ConA-SCHSs on hepatocyte and hepatoma cells. As shown in Fig. S3, there were no significant differences between different concentrations of ConA-SCHSs (500:200, 250:100 and 125:50 μg/mL) or incubation times (6, 12, 18 and 24 hrs). In addition, the ConA-SCHSs did not exert a cytotoxic effect on any of the hepatocyte (NeHepLxHT) and hepatoma (ML-1 and Huh-7) cell lines, even when treatment was carried out with high concentrations (500:200 μg/mL) of ConA with SCHSs for 24 hrs. ConA-SCHSs may thus induce less or even no cytotoxic effects than traditional metal nanoparticles on either normal or cancerous cells.

3.5. The binding capacity of hepatocyte and hepatoma cells with ConA-SCHSs

Flow cytometric analysis was used to compare the binding capacity of hepatocyte (NeHepLxHT) and hepatoma (ML-1 and Huh-7) cells to ConA-SCHSs. Fig. 4A shows that hepatoma (ML-1 and Huh-7) cells have a higher binding capacity than hepatocytes (NeHepLxHT) to ConA-FITC-SCHSs in both 250:100 (59.2±2.6-, 45.6±1.5- and 26.7±1.5-fold for Huh-7, ML-1 and NeHepLxHT cells, respectively) and 125:50 (30.2± 2.8-, 22.3 ± 1.1- and 5.7 ± 0.8-fold for Huh-7, ML-1 and NeHepLxHT cells, respectively) μg/mL of ConA-FITC and SCHSs. Among these two hepatoma cell lines, Huh-7 cells have a higher binding capacity than ML-1 cells with regard to ConA-FITC-SCHSs. Confocal imaging and flow cytometric analysis were performed to verify the binding capacity of cells in relation to ConA-FITC-SCHSs with and without trypsinization of cells, as shown in Fig. 4A. The FITC fluorescence confocal images were taken after the cells were treated with ConA-FITC-SCHSs (250:100 μg/mL) for 12 hrs. As shown in Fig. 4B, most ConA-FITC-SCHSs were close to the plasma membrane, and others were localized in the cytoplasm. The binding capacity of cells to ConA-FITC-SCHSs is significantly higher in both hepatoma cells (ML-1 and Huh-7) than normal hepatocytes (NeHepLxHT). However, ML-1 cells have a higher binding capacity than Huh-7 cells with regard to ConA-FITC-SCHSs. Trypsinization might thus be involved in the binding that occurs between the ConA and ConA receptors on the surface of cells.

3.6. ConA-FITC-SCHSs-mediated photothermal effect

The first biological near-infrared (NIR) window is located in 650-900 nm, which has the maximum depth of penetration in tissue, because of the low absorption of hemoglobin and water.[12] The SCHSs in this study were used as the photothermal agent for hepatocyte and hepatoma cell ablation under irradiation of an 808 nm NIR laser, and then trypan blue staining was performed to identify the dead cells after irradiation. As shown in Figs. 5 and 6, ConA-SCHSs treated hepatoma cells (ML-1 and Huh-7) were more sensitive to NIR irradiation than normal hepatocytes (NeHepLxHT), which

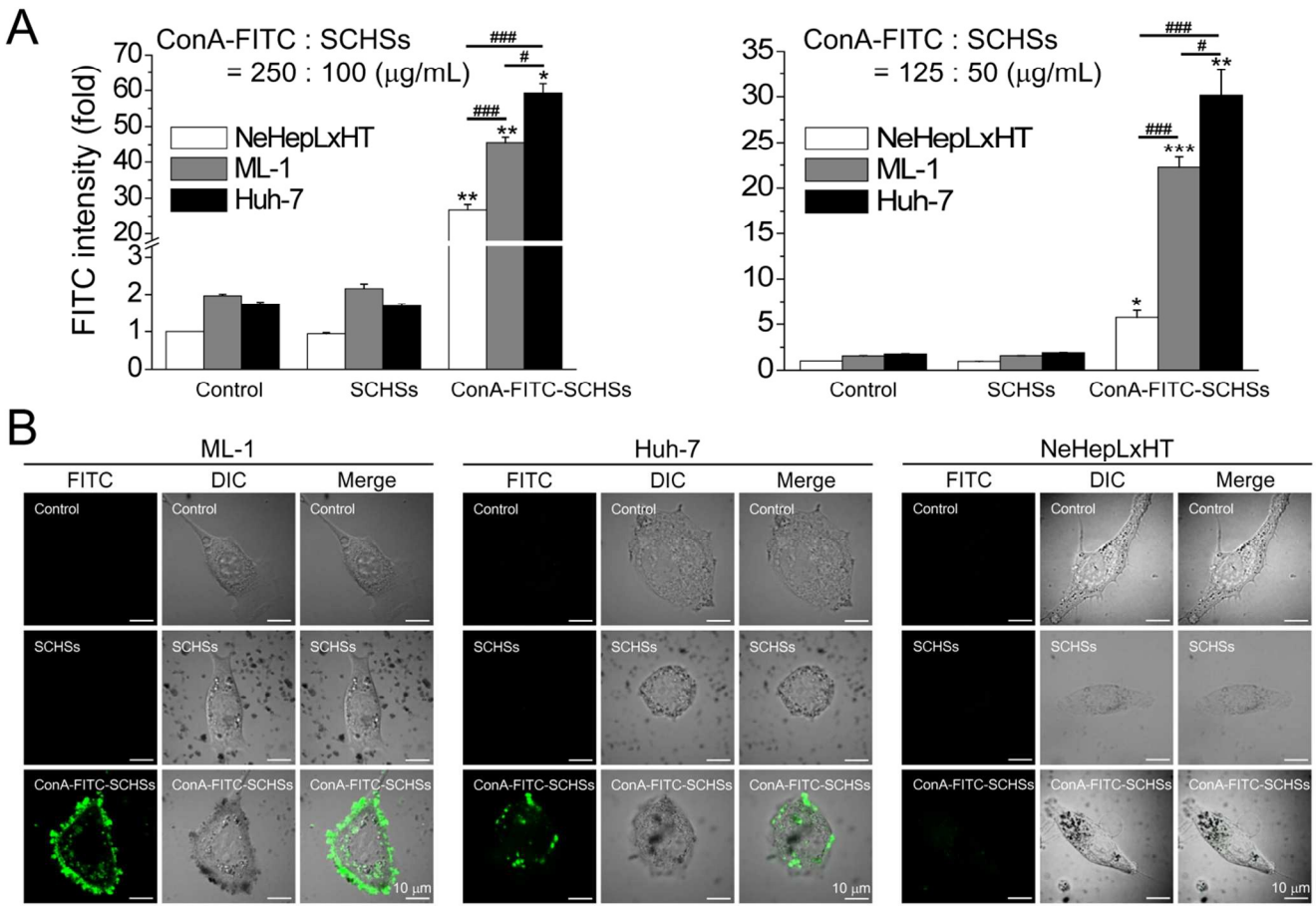

Fig. 4 The binding capacity of different cell type to ConA-FITC-SCHSs. (A) Hepatoma (ML-1, Huh-7) and hepatocyte (NeHepLxHT) cells were incubated with SCHSs only (50 or 100 μg/mL) or ConA-FITC-SCHSs (250:100 or 125:50 μg/mL) for 12 hrs. The binding capacity between cells and SCHSs was performed by flow cytometric analysis. Each column represents mean±SEM from at least five independent experiments. P values were calculated by the Student's t-test: * or #, $p<0.05$; ** or ##, $p<0.01$; *** or ###, $p<0.001$. (B) Hepatoma (ML-1, Huh-7) cells and hepatocyte (NeHepLxHT) cells were incubated with SCHSs only (100 μg/mL) or ConA-FITC-SCHSs (250:100 μg/mL) for 12 hrs. Representative confocal images are shown in FITC fluorescence, DIC and merged images.

might be due to the varied binding capacities between different cells and ConA-SCHSs. Moreover, this kind of photothermal effect on cell viability occurs in a dose-dependent and laser power-dependent manner, which indicates that higher concentrations of ConA-SCHSs (250:100>150:50 μg/mL) and a higher power of the 808 nm NIR laser (250>200>150>100 mW) contributed to significant cell death. Among the hepatoma cells, ML-1 cells are more sensitive than Huh-7 cells to NIR irradiation induced cell death. This is consistent with the results for the binding capacity between ConA-SCHSs and cells, as seen in the confocal images in Fig. 4B. In contrast, no obvious cell death is observed in the control and SCHSs only groups, which were illuminated with different powers of NIR laser. Only a small portion of ML-1 cells died when treated with high concentrations (38.67±23.84% in 250:100 μg/mL and 5.44± 4.26% in 150:50 μg/mL, respectively) of SCHSs only and a high power (250 mW) of NIR irradiation. These findings indicate that ConA is a determining factor that can enhance the binding capacity of SCHSs and cells, and is also related to the SCHSs-mediated photothermal effect with regard to cell death.

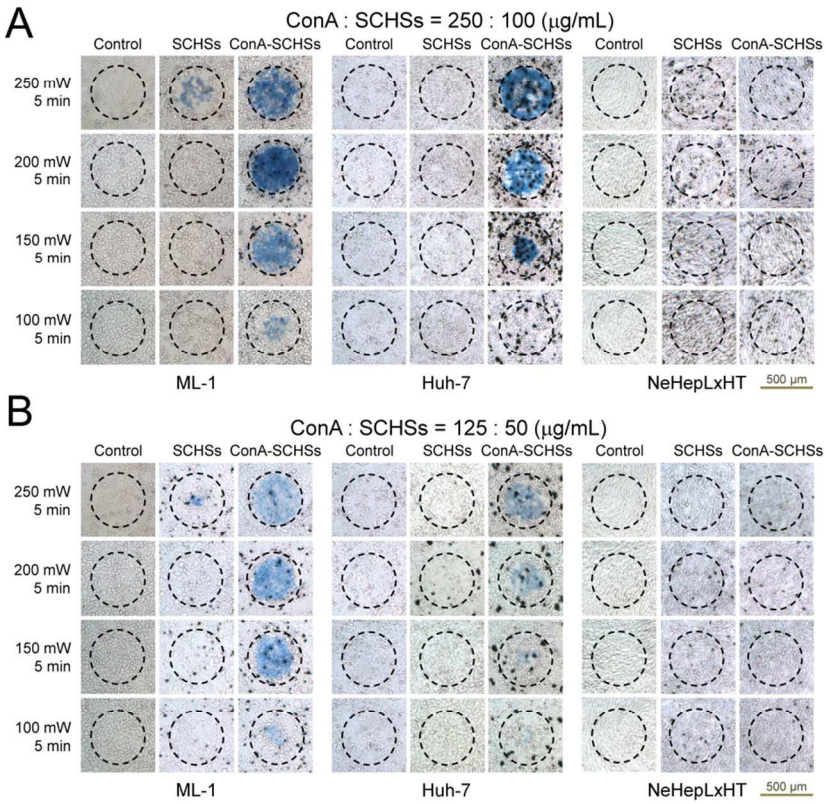

Fig. 5. Photothermal effect of SCHSs on cell ablation. Hepatoma (ML-1, Huh-7) and hepatocyte (NeHepLxHT) cells were incubated with SCHSs only (100 or 50 μg/mL) or ConA-FITC-SCHSs (125:50 or 250:100 μg/mL) for 12 hrs before NIR laser irradiation. Different power levels (100 mW, 150 mW, 200 mW and 250 mW) of NIR laser irradiation were applied to cells for 5 mins. Representative pictures show the blue stained dead cells after trypan blue staining. The dashed circles indicate the irradiation area of the NIR laser spot.

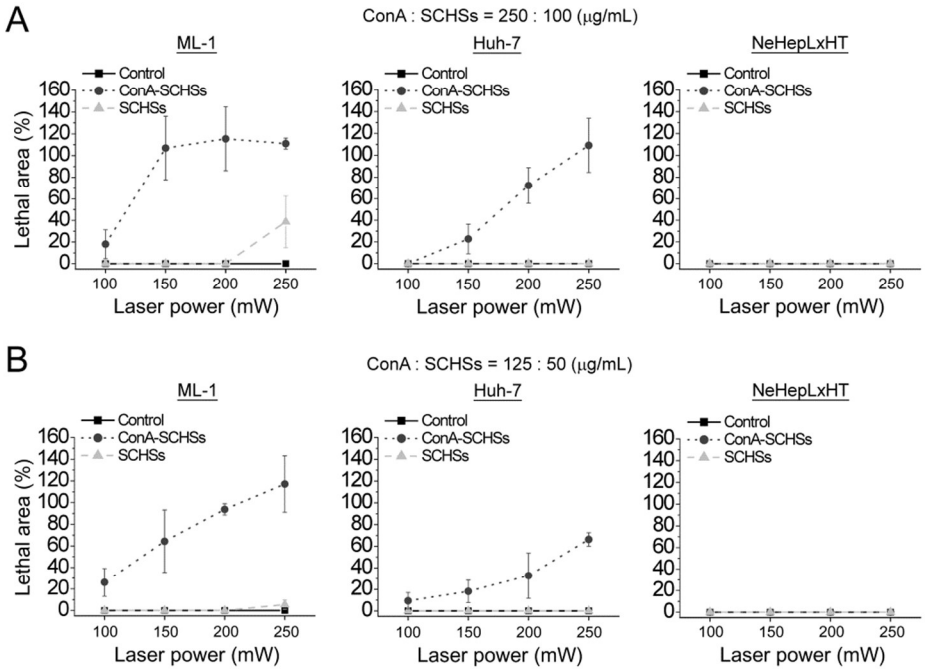

Fig. 6. Photothermal effect of SCHSs on different types of cells. Quantitative analysis of the photothermal effect of SCHSs on cell death in hepatoma (ML-1, Huh-7) and hepatocyte (NeHepLxHT) cells, as described in Fig. 5. The lethal area (%) indicates the area of trypan blue positive stained cells relative to the irradiation area of the NIR laser spot.

Journal of Materials Chemistry B RSCPublishing

PAPER

These results demonstrate that ConA-SCHSs could be an effective NIR photothermal agent to kill cancer cells *in vitro*.

The results of the flow cytometric analysis to measure the binding capacity of ConA-SCHSs to cancerous and normal liver cells are shown in Fig. 4A, and it can be seen that the binding capacity of ConA-SCHSs on cancer cells is greater than that on normal cells. Moreover, similar results were found for the confocal fluorescence images (Fig. 4B) and photothermal ablation capacity (Fig. 6), in that the binding capacity and photothermal ablation effect of ConA-SCHSs on cancer cells are both higher than those on normal cells. However, the flow cytometric analysis showed that the binding capacity of ConA-SCHSs to Huh-7 cells is higher than that to ML-1 cells (Fig. 4A). In contrast, the confocal imaging results show that the binding capacity of ConA-SCHSs to ML-1 cells is higher than that to HuH-7 cells (Fig. 4B). We assume that the contrasting results may be due to the effect of trypsin-EDTA, which disrupts the integrity of ConA receptors, as well as the interaction that occurred between the ConA and ConA receptors due to trypsinization during sample preparation for flow cytometric analysis. To investigate this, cells were treated with ConA-SCHSs before trypsin-EDTA (adherent cells) or after trypsin-EDTA (floating cells) treatment. The results showed that the FITC fluorescence intensity of ConA-FITC-SCHSs in Huh-7 cells in adherent cells (Fig. 3A) was higher than in floating cells (Fig. S4A) after 1 hr incubation. It is thus possible that the flow cytometric analysis results for the trypsin-EDTA treated cells might not fully reflect the binding capacity for cells with ConA-SCHSs. Moreover, the binding capacity for the non-trypsin-EDTA treated cells, as obtained by confocal imaging (Fig. 4B), was consistent with the photothermal ablation capacity (Fig. 6). In addition, ConA-SCHSs did not exert any photothermal effect on NeHepLxHT cells. This can be explained by the fact that the NeHepLxHT cells have less binding capacity to ConA (Figs. 4 and S4A), and their cell volume is larger than that of the ML-1 and Huh-7 cells (Fig. S4B). Therefore, the photothermal effect of SCHSs on NeHepLxHT cells will be reduced.

The results of this study show that the ConA-SCHSs binding capacity and photothermal ablation capacity on hepatoma cells are higher than those on hepatocyte cells. Our results demonstrate that ConA-SCHSs has many important properties with regard to photothermal therapy, including a powerful photothermal effect, high photostability, low cytotoxicity, and good dispensability.

4. Conclusions

In this study we developed biocompatible silica-carbon hollow spheres for use in photothermal therapy under NIR laser irradiation. The average size of the SCHSs was around 300 nm, and we also used ConA, a lectin isolated from *Canavalia ensiformis*, to enhance the binding capacity of SCHSs to specific glycoprotein receptors on the cell surface of liver cancer cells. Flow cytometric assay indicated that different binding capacities of ConA-SCHSs for liver cancer cells and normal liver cells, and confocal microscopy clearly showed that the binding capacity of ConA-SCHSs on the liver cancer cells was higher than that on normal liver cells. The *in vitro* photothermal ablation experiments demonstrated that the ConA conjugated SCHSs killed liver cancer cells efficiently at a relatively low laser power, a finding which may have significance for the treatment of liver cancer. In addition to photothermal effect, the SCHSs could be used as multifunctional agents for drug delivery, gene therapy and photodynamic therapy due to its hollow structural characteristics. An ideal anti-cancer drug delivery system that delivers drugs to cancer cells specifically. Meanwhile, it maintains a constant level of drug over a prolonged period of time. Thus, our developed ConA-SCHSs may have the potential to release anti-cancer drugs in a controllable rate and duration under laser irradiation, especially in liver cancer.

Conflict of interest

The authors declare that they have no conflict of interest.

Acknowledgements

We thank the National Cheng Kung University Medical College Core Research Laboratory, the Clinical Medicine Research Center, and the Micro/Nano Science and Technology Center for supplying technical and equipment. We also thank Prof. H.Y. Lei for his constructive comments on this work.

Notes

[a] Department of Biomedical Engineering, National Cheng Kung University, Tainan 70101, Taiwan

[b] Medical Device Innovation Center, National Cheng Kung University, Tainan 70101, Taiwan

[c] Institute of Biomedical Engineering, National Chiao Tung University, Hsinchu 30010, Taiwan

[d] Department of Chemistry, National Cheng Kung University, Tainan 70101, Taiwan

[e] Institute of Molecular and Cellular Biology, National Tsing Hua University, Hsinchu 30013, Taiwan

[f] Center for Micro/Nano Technology Research, National Cheng Kung University, Tainan 70101, Taiwan

References

1 A. Jemal, F. Bray, M. M. Center, J. Ferlay, E. Ward and D. Forman, *CA Cancer J. Clin.,* 2011**, 61**, 69.

2 M. B. Thomas and A. X. Zhu, *J. Clin. Oncol.,* 2005, **23**, 2892.

3 Á. Juarranz, P. Jaén, F. Sanz-Rodríguez, J. Cuevas and S. González, *Clin. Transl. Oncol.,* 2008, **10**, 148.

4 Y. N. Konan, R. Gurny and E. Allemann, *J. Photochem. Photobiol. B*, 2002, **66**, 89.

5 D. E. Dolmans, D. Fukumura and R. K. Jain, *Nat. Rev. Cancer,* 2003, **3**, 380.
6 B. W. Henderson and T. J. Dougherty, *Photochem. Photobiol.,* 1992, **55**, 145.
7 Z. Zhang, J. Wang and C. Chen, *Adv. Mater.,* 2013, **25**, 3869.
8 S. Lal, S. E. Clare and N. J. Halas, *Acc. Chem. Res.,* 2008, **41**, 1842.
9 M. Nikfarjam, V. Muralidharan and C. Christophi, *J. Surg. Res.,* 2005, **127**, 208.
10 J. P. May and S. D. Li, *Expert Opin. Drug Delivery,* 2013, **10**, 511.
11 W. C. Dewey, *Int. J. Hyperthermia,* 1994, **10**, 457.
12 R. Weissleder, *Nat. Biotechnol.,* 2001, **19**, 316.
13 A. M. Smith, M. C. Mancini and S. Nie, *Nat. Nanotechnol.,* 2009, **4**, 710.
14 G. W. Hart and R. J. Copeland, *Cell,* 2010, **143**, 672.
15 B. Liu, C. Y. Li, H. J. Bian, M. W. Min, L. F. Chen and J. K. Bao, *Arch. Biochem. Biophys.,* 2009, **482**, 1.
16 W. W. Li, J. Y. Yu, H. L. Xu and J. K. Bao, *Biochem. Biophys. Res. Commun.,* 2011, **414**, 282.
17 G. M. Edelman, B. A. Cunningham, G. N. Jr. Reeke, J. W. Becker, M. J. Waxdal and J. L. Wang, *Proc. Natl. Acad. Sci. U.S.A.,* 1972, **69**, 2580.
18 H. Y. Lei and C. P. Chang, *J. Biomed. Sci.,* 2009, **16**, 10.
19 X. Huang, I. H. El-Sayed, W. Qian and M. A. El-Sayed, *J. Am. Chem. Soc.,* 2006, **128**, 2115.
20 X. Huang, P. K. Jain, I. H. El-Sayed and M. A. El-Sayed, *Lasers Med. Sci.,* 2008, **23**, 217.
21 B. Van de Broek, N. Devoogdt, A. D'Hollander, H. L. Gijs, K. Jans, L. Lagae, S. Muyldermans, G. Maes and G. Borghs, *ACS Nano,* 2011, **5**, 4319.
22 J. K. Young, E. R. Figueroa and R. A. Drezek, *Ann. Biomed. Eng.,* 2012, **40**, 438.
23 C. Iancu and L. Mocan, *Int. J. Nanomedicine,* 2011, **6**, 1675.
24 Z. M. Markovic, L. M. Harhaji-Trajkovic, B. M. Todorovic-Markovic, D. P. Kepic, K. M. Arsikin, S. P. Jovanovic, A. C. Pantovic, M. D. Dramicanin and V. S. Trajkovic, *Biomaterials,* 2011, **32**, 1121.
25 H. Yang, C. Liu, D. Yang, H. Zhang and Z. Xi, *J. Appl. Toxicol.,* 2009, **29**, 69.
26 X. Yang, J. Liu, H. He, L. Zhou, C. Gong, X. Wang, L. Yang, J. Yuan, H. Huang, L. He, *et al.*, *Part. Fibre Toxicol.,* 2010, **7**, 1.
27 C. Y. Chang-Chien, C. H. Hsu, T. Y. Lee, C. W. Liu, S. H. Wu, H. P. Lin, C. Y. Tang and C. Y. Lin, *Eur. J. Inorg. Chem.,* 2007, **24**, 3798.
28 Y. Reid, J. P. Gaddipati, D. Yadav and J. Kantor, *In Vitro Cell. Dev. Biol.: Anim.,* 2009, **45**, 535.
29 D. F. Gilbert, G. Erdmann, X. Zhang, A. Fritzsche, K. Demir, A. Jaedicke, K. Muehlenberg, E. E. Wanker and M. Boutros, *PLoS ONE,* 2011, **6**, e28338.
30 J. McCarthy, J. Friel and P. Camus, *Microsc. Microanal.,* 2009, **15**, 484.
31 S. Mitragotri and J. Lahann, *Nat. Mater.,* 2009, **8**, 15.

